JOURNAL OF AIRCRAFT
Vol. 32, No. 6, November–December 1995

# Flat Spin of Axisymmetric Bodies

L. E. Ericsson*
*Mt. View, California 94040*
and
M. E. Beyers†
*Institute for Aerospace Research, Ottawa, Ontario K1A 0R6, Canada*

**Experimental results are analyzed to develop an understanding of the flow physics causing flat spin of axisymmetric bodies, which is a key to the development of the capability for the prediction of the flat spin of advanced aircraft. The flow phenomenon sustaining the flat spin motion is the flow separation asymmetry due to the moving wall effect at locally critical flow conditions on the body, which is made possible by the presence of three-dimensional flow effects. Body roughness and microasymmetry play important roles in extending the range of ambient flow conditions at which flat spin can develop.**

## Nomenclature

$D$ = maximum body diameter
$d$ = local body diameter
$L'$ = sectional lift, coefficient $c_l = L'/(\rho_\infty U_\infty^2/2)d$
$l$ = body length
$N$ = flat spin rate
$n$ = yawing moment, coefficient $C_n = n/(\rho_\infty U_\infty^2/2)Sl$
$P$ = static pressure, coefficient $C_p = (P - P_\infty)/(\rho_\infty U_\infty^2/2)$
$p$ = rotation rate of circular cross section
$Re$, $Re_\infty$ = Reynolds number, $U_\infty d/\nu_\infty$, $U_\infty D/\nu_\infty$, respectively
$S$ = reference area, $\pi D^2/4$
$t$ = time
$U$ = velocity
$V$ = total cross-sectional velocity
$x$ = axial body-fixed coordinate
$Y'$ = sectional side force, coefficient $c_y = Y'/(\rho_\infty U_\infty^2/2)d$
$y$ = coordinate orthogonal to $x$ and rotation axes
$\alpha$ = angle of attack
$\Delta$ = increment
$\delta$ = roughness height
$\nu$ = kinematic viscosity
$\rho$ = fluid density
$\Phi$ = body roll angle
$\Omega$ = dimensionless spin rate, $Nl/2U_\infty$

*Subscripts*

cg = center of rotation
cr = critical
FS = flat spin
max = maximum
$W$ = wall
$\infty$ = freestream conditions

Presented as Paper 94-0168 at the AIAA 32nd Aerospace Sciences Meeting and Exhibit, Reno, NV, Jan. 10–13, 1994; received Aug. 8, 1994; revision received March 16, 1995; accepted for publication April 26, 1995. 

*Engineering Consultant. Fellow AIAA.
†Head Aircraft Aerodynamics Group, Aerodynamics Laboratory. Senior Member AIAA.

## Introduction

THE steadily increasing demand on aircraft agility has focused attention on high-alpha vehicle dynamics, including departure and flat-spin characteristics. A recent Department of Defense release of the statistics for F-14 spins illustrates the need for a better understanding of flat-spin aerodynamics[1] (Fig. 1). The most likely reason for the observed occurrence of the flat spin is that the large control-induced yaw rate generated a side force and an associated increase of the normal force[2] on the slender forebody that caused departure and drove the aircraft into a flat-spin motion. Since the dominant contribution to the forces acting on a high-performance aircraft in flat spin are generated on the forebody, such as the slender nose in Fig. 1, it is appropriate to analyze the flat-spin behavior of bodies of revolution. The purpose of this article is to examine available experimental and theoretical results in order to pinpoint the flow physics behind this behavior for bodies of revolution.

## Background

At high angles of attack the asymmetric flow separation occurring on a slender body of revolution generates large asymmetric loads.[2] When the body is in lateral motion, the so-called moving wall effect[3] governs the dynamics of the flow

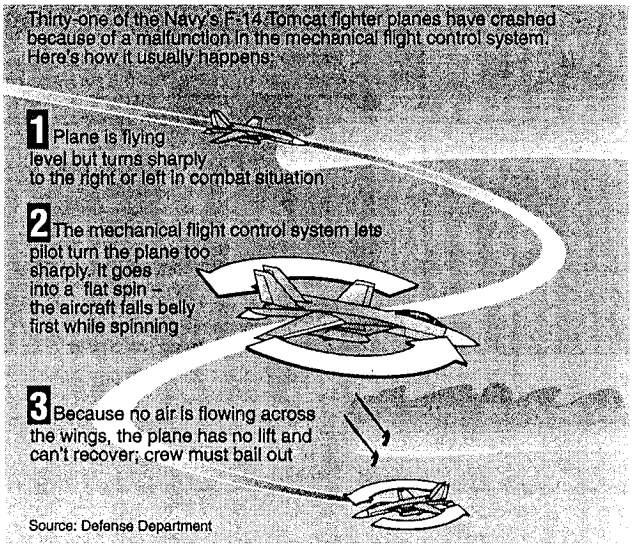


**Fig. 1 How the F-14 spins out of control.[1]**

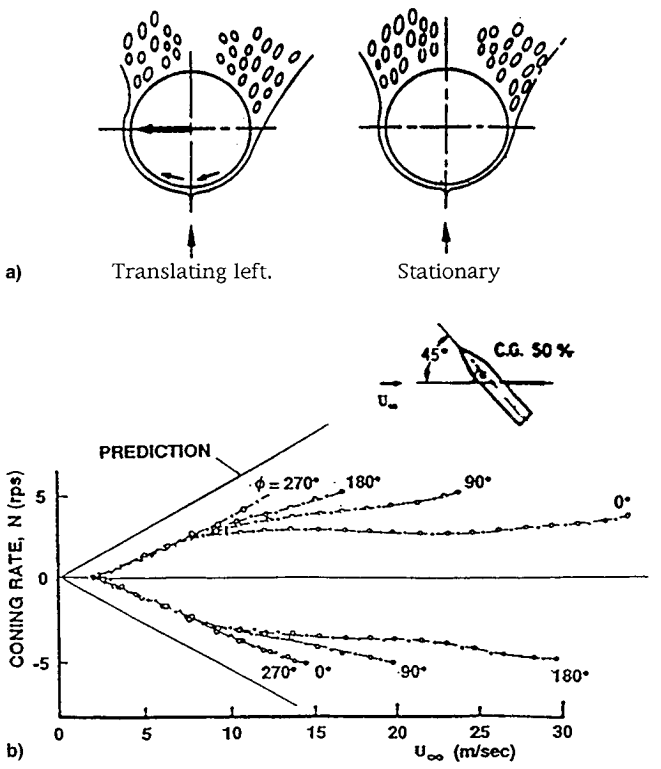


Fig. 2 Moving wall effects on a coning cone-cylinder: a) translating circular cross section and b) cone-cylinder coning at $\alpha = 45$ deg.

separation (Fig. 2a). This viscous-flow/motion coupling can drive the body in a coning motion. The power of the moving wall effects is well illustrated by the results of a free-to-spin experiment at $\alpha = 45$ deg of a cone-cylinder configuration[4] (Fig. 2b), showing that moving wall effects dominated over the static asymmetry.[2] It has been demonstrated[5] that for a slender body coning at high angles of attack, the moving wall effect can be analyzed by applying the Magnus lift results for a rotating circular cylinder.[6] This follows from the observation that the moving wall effects for the translating cross section of the coning body (Fig. 2a) are largely the same as for the rotating circular cylinder[6] (Fig. 3), because the relevant moving wall effects are those concentrated in a region near the flow stagnation point, where the boundary-layer buildup starts.[7]

In the case of flat spin there are some similarities with the coning case. However, the basic flow physics are different. For coning as well as flat-spin motions of a perfectly smooth axisymmetric body the initial spin-producing moment would be determined by external perturbations of some sort, such as flow nonuniformity or unsteadiness. Even if the spin axis were located at the geometrical centroid, the side forces would not be balanced on the two sides of the axis in the presence of a nonuniform roughness distribution or facility-induced flow asymmetry.[8] Once the flat spin is initiated, moving wall effects apparently play the same dominant role as in the case of the coning motion[4,5] at $\alpha < 90$ deg. This can be appreciated from the results for a circular cylinder.[9-12] Judging by the pressure measurements on a circular cylinder[9] driven at 500 rpm around the midbody axis at $Re = 0.318 \times 10^6$, the local rotation-induced effects produced the supercritical/critical, one-bubble[10] flow separation asymmetry in opposite directions on

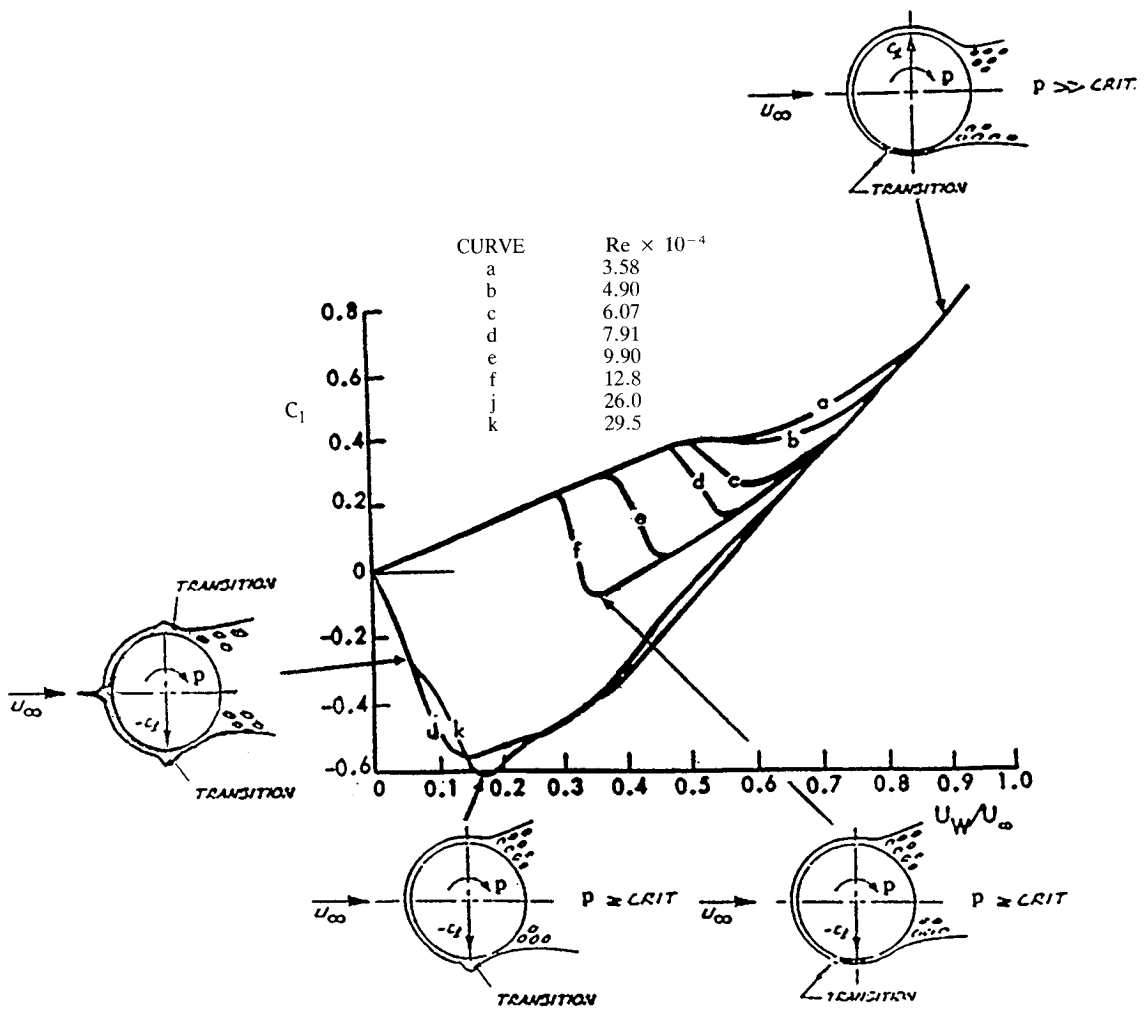


Fig. 3 Magnus lift of rotating circular cylinder.[6]

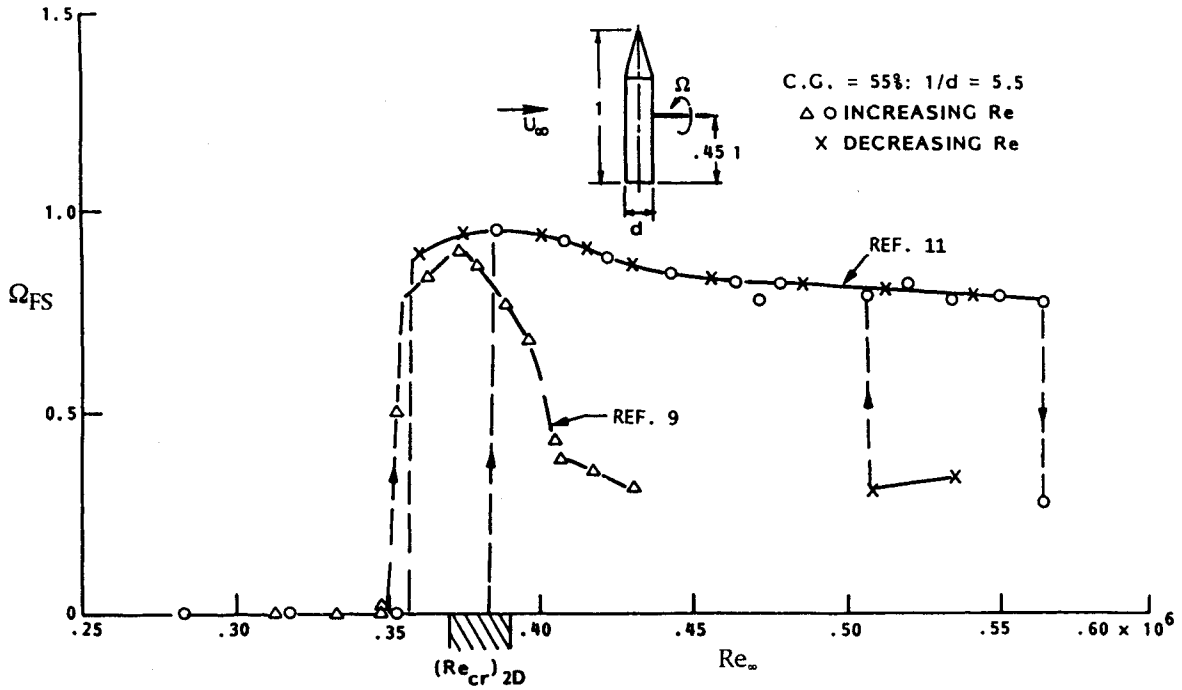


**Fig. 4 Flat spin of an $l/D$ = 5.5 cone-cylinder body.**

the two sides of the rotation axis. As this will generate a pro-spin yawing moment, it is clear how the observed steady-state flat spin[9,11] (Fig. 4) was maintained.[12,13]

## Flow Physics

It is important to identify the flow phenomena in flat spin[9,11] (Fig. 4) and to determine how they differ from those for coning.[4,5] One observes that in the case of coning (Fig. 2b) the spin-up occurs as long as the crossflow conditions are subcritical, whereas the flat spin (Fig. 4) is initiated only at critical crossflow conditions. The purpose of the present analysis is to try to pinpoint the flow physics causing steady-state flat spin.

### Moving Wall Effect

The moving wall effect becomes extremely large at critical flow conditions, when it affects flow separation via boundary-layer transition. This is demonstrated by the two-dimensional Magnus lift characteristics[6] shown in Fig. 3. At $Re = 0.128 \times 10^6$, increasing $p$ above the critical value, giving $U_W/U_\infty \geq 0.3$ (curve f in Fig. 3), results in Magnus lift reversal. The upstream moving wall effect on the bottom side causes transition of the laminar boundary layer, changing the flow separation from the subcritical towards the supercritical type. This results in an almost instantaneous loss of lift, $\Delta c_l \approx -0.3$. When the Reynolds number is increased to the critical value, $Re \approx 0.3 \times 10^6$ (curves j and k in Fig. 3), the moving wall effect acts on the shear-layer transition in the laminar separation bubble, greatly increasing the magnitude of the Magnus lift reversal, $\Delta c_l \approx -0.6$ compared to $\Delta c_l \approx -0.3$. Comparing the negative Magnus-lift slope for curves j and k in Fig. 3 with the positive slope at $U_W/U_\infty < 0.3$ for curves a–f, one gets an appreciation for how much more powerful the moving wall effect is at critical than at subcritical flow conditions.

Similar behavior is illustrated for the three-dimensional case by Polhamus' experimental results.[14] It can be seen in Fig. 5 that using static $c_y$ values in a strip analysis gives a rather good prediction of the flat-spin (yawing) moment $C_n$ as a function of the reduced spin rate $\Omega = Nl/2U_\infty$ for subcritical and supercritical flow conditions. For the midbody rotation axis, $\Omega = (U_W)_{max}/U_\infty$. However, in the critical flow region, where viscous moving wall effects are dominant,[3] the measured $C_n$ cannot be predicted by using static data. For the two-dimensional case in Fig. 3, at $U_W/U_\infty < 0.1$, the moving wall effect delays transition in the laminar separation bubble on the top side and promotes it on the bottom side. As a consequence, the final turbulent flow separation is delayed more on the bottom side than on the top side, resulting in the measured negative Magnus lift (Fig. 3). In the flat-spin case[14] (Fig. 5), the moving wall effect on the two-bubble separation geometry will also generate a negative lift force, generating a cross-sectional force opposite to the direction of the motion, thereby creating a damping, antispin yawing moment, as is illustrated in Fig. 6 for $\Omega < 0.25$. Note that the drag-generated contribution to $C_n$ is of much smaller magnitude at critical than at subcritical flow conditions.[12] Consequently, the antispin moment $C_n$ in Fig. 6 for $\Omega < 0.25$ is largely generated by the critical/critical crossflow separation. Comparing Fig. 6 with Fig. 3, one concludes that in the three-dimensional case (Fig. 6), there is a complicated flow mech-

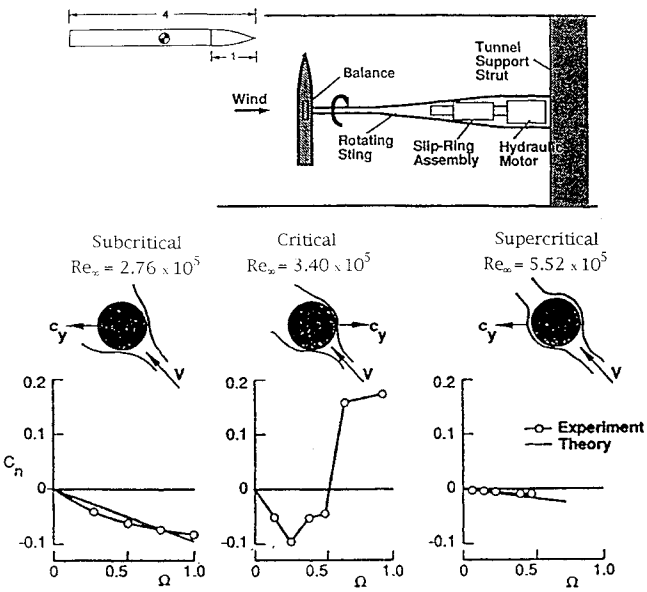


**Fig. 5 Flat spin test of an ogive-cylinder body.[14]**

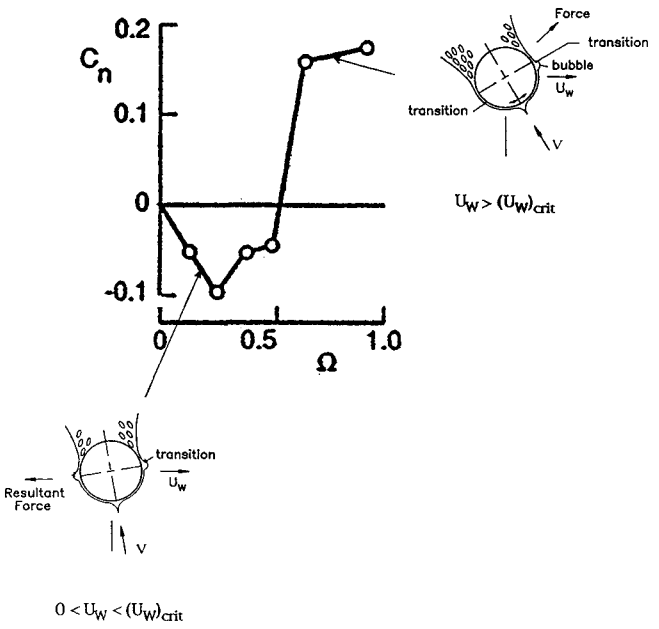


**Fig. 6 Yawing moment for forced flat spin at critical flow conditions.[14]**

anism that involves transition from the two-bubble to the final one-bubble supercritical–critical separation geometry, that generates the pro-spin sectional side force[13] [insert for $U_W > (U_W)_{crit}$ in Fig. 6] responsible for the large positive $C_n$ at $\Omega > 0.5$. This pro-spin component of the moment decreases with increasing spin-rate-induced skewing of the crossflow, as illustrated in Fig. 6, causing $C_n$ to level off at higher rotation rates. Also contributing to this data trend is the outboard movement of the critical flow region with increasing spin rate.

The $C_n$ results in Figs. 5 and 6 illustrate the fact that for the free-to-spin case a large static moment is needed to drive the axisymmetric body through the low $\Omega$ range. However, once $\Omega > 0.5$, the moving wall effect will generate the supercritical–critical crossflow separation that produces the pro-spin moment needed to maintain flat spin (Fig. 6).

### Roughness Effects

The presence of flow separation asymmetry below the critical flow conditions for a smooth body of revolution is likely to be the result of nonuniform roughness distribution. This is apparent from the flat-spin results for a cone-cylinder[9,11] shown in Fig. 4. The poor agreement between the results from Refs. 9 and 11, with the spin-up occurring at a Reynolds number below the critical in the test of Ref. 9, was apparently caused by roughness effects.[15] When the model used in Ref. 9 was polished, the results agreed with those in Ref. 11. Roughness caused the critical flow condition to be encountered earlier in the original test of Ref. 9. Consequently, the most likely reason for the flat spin starting below the critical flow regime in that test,[9] at $Re < (Re_{cr})_{2D}$ in Fig. 4, is a nonuniform side-force distribution caused by unevenly distributed roughness. Uniform roughness has been shown to inhibit the flat-spin development[9] (Fig. 7). In Ref. 13 it is demonstrated that it is the supercritical/critical crossflow separation [insert for $U_W > (U_W)_{crit}$ in Fig. 6] that produces the final limiting rate of the flat spin on a circular cylinder. When considering the effect of roughness on the Reynolds number boundaries of the critical flow region[16] (Fig. 8), one finds that even with the definition of smooth suggested by Schechenyi,[17] i.e., $(\delta/d)_{smooth} = 3.3 \times 10^{-4}$, the critical region extends from $Re = 1.8 \times 10^5$ to $Re = 5.7 \times 10^5$. The figure illustrates how extremely sensitive the boundaries of the critical flow region are to roughness.

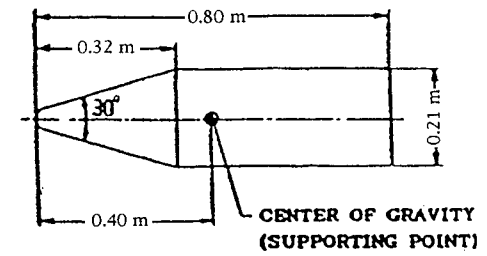


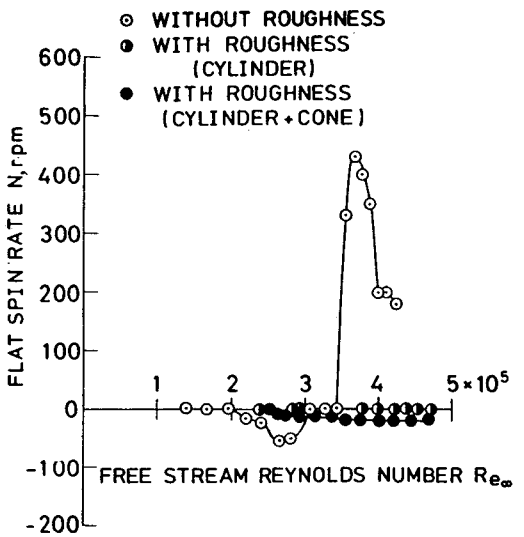


**Fig. 7 Alleviation of flat spin with sandpaper roughness.[9]**

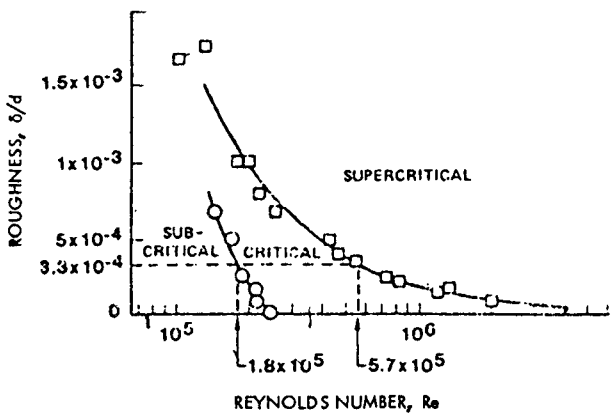


**Fig. 8 Effect of roughness on the critical Reynolds number range.[16]**

### Unsteady Vortex Shedding

When comparing the results in Fig. 4 for $\alpha = 90$ deg with the coning results[4,5] in Fig. 2b for $\alpha = 45$ deg, the following question arises: for subcritical flow conditions, why are the undamping moving wall effects causing the steady-state coning absent in the flat-spin case? One important difference is that unsteady Kármán vortex shedding is present only for the flat-spin case. The oscillatory forces due to Kármán vortex shedding at subcritical flow conditions have been found to be of the same magnitude as the measured Magnus lift on a rotating circular cylinder.[6,18] For the rotating circular cylinder in Fig. 3, the steady moving wall effects are apparently strong enough to rotate the flow separation to produce a nonzero time average in the presence of Kármán vortex shedding. This occurs because the moving wall effects interact with the boundary layer up to the flow separation point. In contrast, on the cylinder in flat spin the moving wall effects are of the translational type, concentrated in the boundary-layer buildup region near the flow stagnation point, and cannot compete

with the forced oscillation of the separation point through Kármán vortex shedding,[7,19] resulting in zero time-averaged side force. A similar condition exists at supercritical flow conditions. However, the classic type of Kármán vortex shedding with a unique Strouhal number found at subcritical or supercritical flow conditions does not exist for critical flow conditions,[20] where flat spin occurs. When the moving wall effects are not of the oscillatory type that causes lock-on,[7] they will tend to suppress Kármán vortex shedding rather than enhance it, thereby allowing flat spin to occur.

**Three-Dimensional Flow Effects**

Another obvious difference between coning and flat spin is that on the coning body the axial flow component provides the venting of the separated flow region that is needed to establish steady asymmetric flow separation at all Reynolds numbers,[2] whereas in flat spin it is only in the critical Reynolds number range that an asymmetric flow separation geometry can be established. Under these conditions it is likely that an open laminar separation bubble is established on each half-span of the rotating cylinder, locked in position by the spanwise variation of local Reynolds number and pressure gradient (Fig. 9). The separation bubbles will be vented by a spiral vortex leaving the surface and rolling up with the tip vortex system. The fact that the experimentally observed[9] two-level flat spin in Fig. 10 developed only for $x_{c.g.} = 0.50$ may suggest that for $x_{c.g.} = 0.69$ the cylindrical, flat-based part was too short to support the flow geometry sketched in Fig. 9.

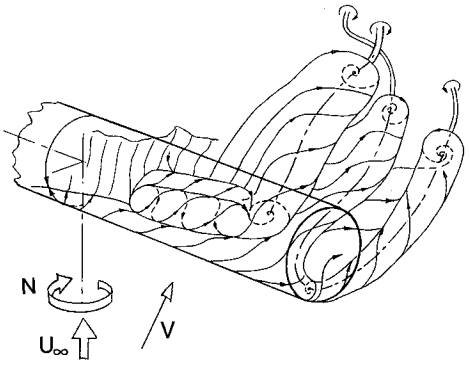


**Fig. 9 Conjectured flowfield on a circular cylinder in flat spin at critical Reynolds numbers.[13]**

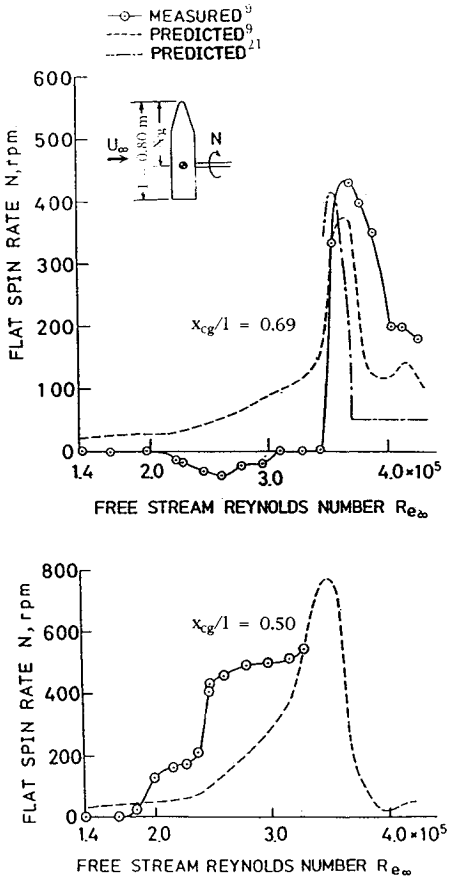


**Fig. 10 Effect of rotation-axis location on the flat spin of a cone-cylinder.[9]**

Figure 10 shows the results of two attempts[9,21] to predict the experimental results.[9] The method of Ref. 9 uses the measured static yawing moment as an input, whereas the method of Ref. 21 uses static two-dimensional measurements of lift and drag on a circular cylinder to determine the sectional force coefficients. The yawing moment is obtained through a strip analysis in which the sectional coefficients have been modified to account for the spanwise variation of the local Reynolds number through the spin-induced local velocity. The sectional forces are then obtained by use of the local dynamic pressure ($\rho_\infty V^2/2$), including the effect of the spin-induced velocity component. It can be seen that the predictions based upon static experimental results do not agree with the dynamic experimental data trends. The problem is the same as that encountered when trying to simulate dynamic stall conditions.[22] Simulating the velocity vector geometry at the edge of the boundary layer only assures similarity for inviscid flow conditions, not for viscous flow. Moreover, important three-dimensional flow effects are neglected in these analyses.

When the rotation axis is at midbody, $x_{c.g.} = 0.50$ in Fig. 10, the cylindrical portion of the model supplies the dominant side forces, causing flat spin when the Reynolds number is increased to $Re_\infty \geq 2 \times 10^5$. The results are similar to those for a circular cylinder,[14] discussed in Ref. 13, but with two flat-spin levels developing in this case. This occurs because the spin-induced supercritical–critical local flow separation will be established first on the blunt-based end of the cylinder, and only later, at a higher $Re$, on the cone-tipped end of the cylinder. Note that the moment on the blunt-based end will continue to drive the flat spin at $Re > Re_{cr}$ (see Fig. 4). When the rotation center was moved to $x_{c.g.} = 0.69$, the loads on the conical nose became dominant due to the longer lever arm. As a result, the Reynolds number based upon the model diameter had to be increased to $Re_\infty \geq 3.4 \times 10^5$ before the flow conditions on the nose became critical. In both cases, $x_{c.g.} = 0.50$ and 0.69, a combination of local roughness and local crossflow Reynolds number determines the spanwise locations of the regions with critical flow conditions. With $Re = Re_\infty[1 + 4(x_{c.g.} - x)^2\Omega^2]^{1/2}$, the following conditions are obtained at the base of the conical nose when $x_{c.g.} = 0.69$ and $N = 450$ rpm: $Re_{max} = 4.35 \times 10^5$ for $Re_\infty = 3.5 \times 10^5$. That is, $Re = 2.9 \times 10^5$ at the centroid of the nose, which is within the critical range as shown by the results for the cylindrical afterbody for $x_{c.g.} = 0.50$ and $N > 200$ rpm.

A strong tip vortex does not exist on the pointed nose of an axisymmetric body at $\alpha = 90$ deg, and the spanwise flow

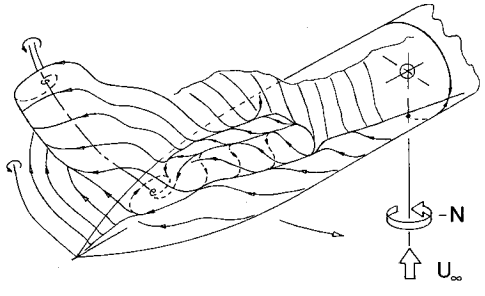


**Fig. 11 Conjectured flow separation on an axisymmetric body with pointed nose in flat spin at critical flow conditions.**

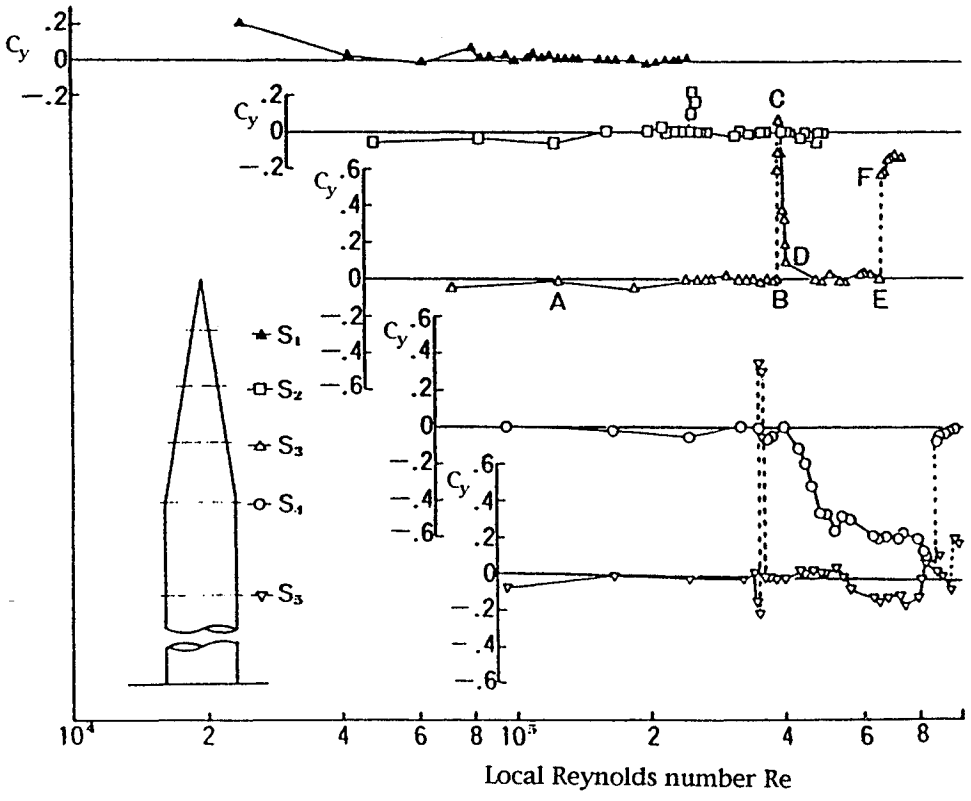


Fig. 12 Measured side force on slender cone-cylinder.[23]

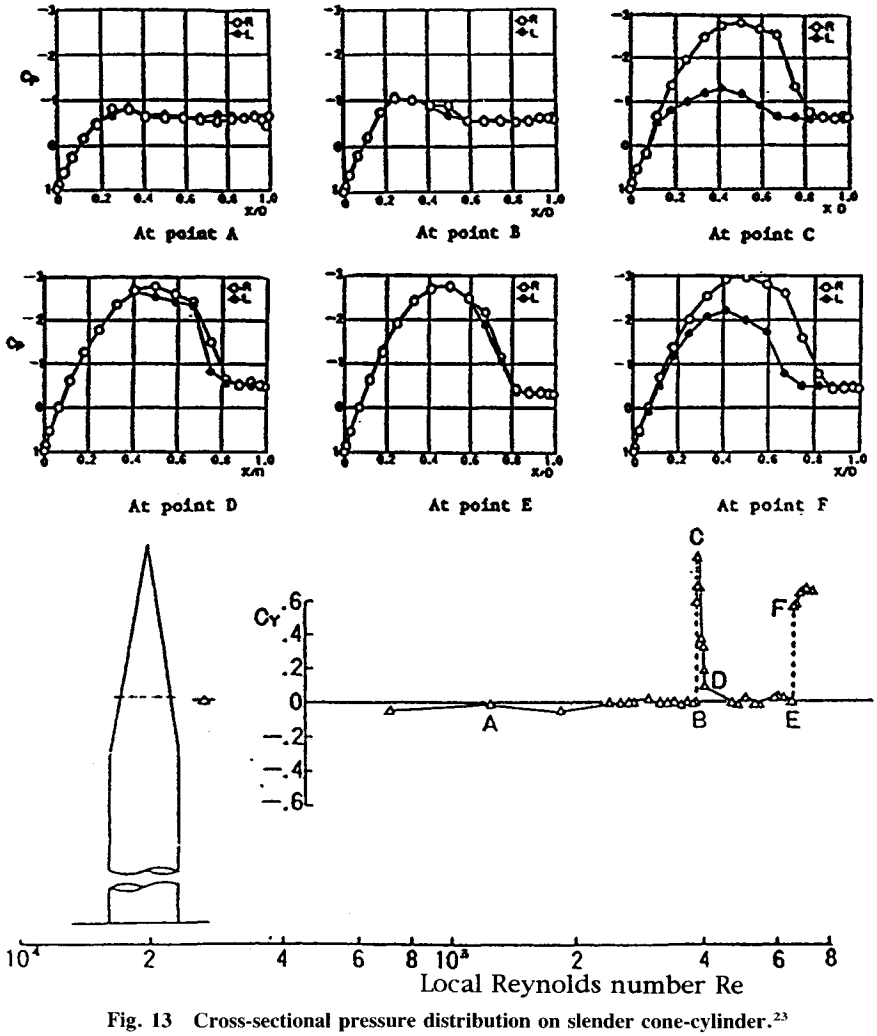


Fig. 13 Cross-sectional pressure distribution on slender cone-cylinder.[23]

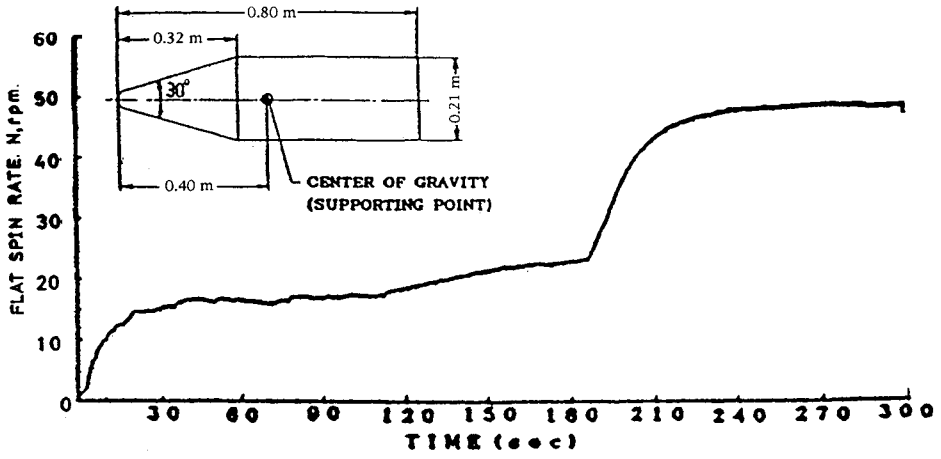


**Fig. 14 Transient flat spin characteristics of cone-cylinder.[24]**

component near the flow stagnation line is stronger than that for a cylindrical body[13] because of the tapering contour, which assists the spanwise venting of the flow separation (Fig. 11). Therefore, a helically skewed, open separation bubble could exist on part of the pointed section even when the center of rotation is quite far forward. Since it will not be restrained by a tip vortex system such as that shown in Fig. 9 the laminar separation bubble could extend outboard of the nose-cylinder shoulder. In this case the focus of separation will be locked into position by the laminar flow separation region near the tip, thereby eliminating the side force near the tip. That is why the cylindrical section provides the dominant driving force for $x_{c.g.} = 0.50$ in Fig. 10. On the other hand, for $x_{c.g.} = 0.69$, in addition to having a longer lever arm, the pointed nose may be alone in being able to support a laminar separation bubble (Fig. 11).

#### Flat-Spin Results

In the case of the flat spin of an advanced aircraft[1] (Fig. 1), one must know what the unsteady separated flow characteristics are on the slender forebody. In that regard the static test results for a 5.4-deg cone-cylinder at $\alpha = 90$ deg (Ref. 23 and Fig. 12) are of great interest. Figure 12 shows that the Reynolds number based upon the local diameter is a rather good indicator of when the asymmetric loads will first occur. Section $S_1$ near the apex appears to be an exception to this rule, showing no measurable side force at critical flow conditions. Section $S_2$ appears to have a small side force at the critical Reynolds number. The more pronounced three-dimensional flow effects near the tip could possibly account for the lower $Re_{cr}$ for section $S_2$.

Of particular interest is the large Reynolds number range over which a significant side force is generated at the cone-cylinder shoulder, section $S_4$. This suggests that asymmetric crossflow separation, such as the supercritical–critical type shown in the sketch for $U_W > (U_W)_{crit}$ in Fig. 6, could be established over a significant spanwise extent on both sides of the nose-cylinder shoulder, in agreement with the flow picture sketched in Fig. 11. Also of considerable interest is the occurrence of a second $c_y$ peak at higher Reynolds number in sections $S_3$ and $S_5$. Pressure distributions in section $S_3$ (Fig. 13) show that the first $c_y$ peak, point C at $Re = 4.0 \times 10^5$, is caused by the subcritical/critical separation geometry. In the static case in Fig. 13, $c_y$ can go in either direction. However, in the flat-spin case, it establishes itself in a direction opposite to that of the motion producing an antispin yawing moment. The separation bubble would be created on the upstream side, whereas laminar separation would occur on the downstream side. Just before the second $c_y$ peak, at point E, the symmetric, critical/critical separation geometry is established, which also generates an antispin moment, as was discussed in connection with Fig. 6 for $\Omega < 0.5$. At the following $c_y$ peak, at point F, the supercritical/critical separation geometry is finally established [generating the prospin moment that drives the flat spin insert for $U_W > (U_W)_{crit}$ in Fig. 6].

In the case of the very peculiar flat-spin results[24] shown in Fig. 14, it appears that the initial spin-up started because the static separation asymmetry[13] was established over some spanwise segment on the cylindrical portion (Fig. 12). As illustrated in Figs. 12 and 13, two or more crossflow separation geometries of the subcritical–critical, critical–critical, and supercritical–critical types can coexist. If this is the case for the geometry in Fig. 14 the slow spin-up at $t > 30$ s from $N \approx 15$ rpm to slightly above 20 rpm could be due to an antispin moment contribution from a separation region on the cone-cylinder with subcritical–critical or critical–critical crossflow separation. When the spin rate reaches the value for which the local Reynolds number on the cone becomes high enough to generate a significant region with supercritical–critical crossflow separation, the rapid spin-up to the final flat-spin rate $N \approx 50$ rpm seen at $t > 180$ s in Fig. 14 would occur.

## Conclusions

An examination of existing experimental results for the flat spin of slender bodies of revolution indicates that a very large yawing moment can be developed on a long slender forebody, capable of driving the flat spin of an advanced aircraft.

1) As has been shown to be the case for a circular cylinder, flat spin is maintained by a supercritical/critical crossflow separation asymmetry generated by moving wall effects.

2) The flow mechanism driving flat spin is made possible by three-dimensional flow effects that provide spanwise venting of the asymmetrical flow separation.

3) Development of more than one threshold of the flat spin rate is attributed to the progressive establishment of critical flow regimes at different spanwise locations.

## References

[1]Thompson, M., "Tendency to Spin Caused Crash of 31 F-14s, Navy Says," *San Jose Mercury News*, April 6, 1993, p. 6A.

[2]Ericsson, L. E., and Reding, J. P., "Asymmetric Flow Separation and Vortex Shedding on Bodies of Revolution," *Tactical Missile Aerodynamics: General Topics*, edited by M. J. Hemsch, Vol. 141, Progress in Astronautics and Aeronautics, AIAA, Washington, DC, 1992, pp. 391–452, Chap. 10.

[3]Ericsson, L. E., "Moving Wall Effects in Unsteady Flow," *Journal of Aircraft*, Vol. 25, No. 11, 1988, pp. 977–990.

[4]Yoshinaga, T., Tate, A., and Inoue, K., "Coning Motion of Slender Bodies at High Angles of Attack in Low Speed Flow," AIAA Paper 81-1899, Aug. 1981.

[5]Ericsson, L. E., "Prediction of Slender Body Coning Characteristics," *Journal of Spacecraft and Rockets*, Vol. 28, No. 1, 1991, pp.

43–49.

[6]Swanson, W. M., "Magnus Effect: A Summary of Investigations to Date," *Journal of Basic Engineering*, Vol. 83, Sept. 1961, pp. 461–470.

[7]Ericsson, L. E., "Circular Cylinder Response to Kármán Vortex Shedding," *Journal of Aircraft*, Vol. 25, No. 9, 1988, pp. 769–775.

[8]Beyers, M. E., and Ericsson, L. E., "Ground Facility Interference on Aircraft Configurations with Separated Flow," *Journal of Aircraft*, Vol. 30, No. 5, 1993, pp. 682–688.

[9]Kubota, H., Irai, I., and Matsuaka, M., "Wind Tunnel Investigations for the Flat Spin of Slender Bodies at High Angles of Attack," *Journal of Spacecraft and Rockets*, Vol. 20, No. 2, 1983, pp. 108–114; also AIAA Paper 82-0054, Jan. 1982.

[10]Bearman, P. W., "On Vortex Shedding from a Circular Cylinder in the Critical Reynolds Number Regime," *Journal of Fluid Mechanics*, Vol. 37, Pt. 3, 1969, pp. 577–585.

[11]Yoshinaga, T., and Tate, A., private communication, Dec. 20, 1985.

[12]Ericsson, L. E., "Flat Spin of Axisymmetric Bodies in the Critical Flow Region," *Journal of Spacecraft and Rockets*, Vol. 24, No. 6, 1987, pp. 532–538.

[13]Ericsson, L. E., and Beyers, M. E., "On the Flat Spin of a Circular Cylinder," AIAA Paper 94-0158, Jan. 1994.

[14]Ericsson, L. E., and Beyers, M. E., "Viscous-Flow/Vehicle-Motion Coupling," *Fluid Dynamics of Rotary Flows, Rotary-Balance Testing for Aircraft Dynamics*, AGARD-AR-265, Dec. 1990, pp. 164–167, 183–187, Chap. 8.

[15]Kamiya, N., Suzuki, S., and Nishi, T., "On the Aerodynamic Force Acting on a Circular Cylinder in the Critical Range of the Reynolds Number," AIAA Paper 79-1475, July 1979.

[16]Schlinker, R. H., Fink, M. R., and Amiet, R. K., "Vortex Noise from Non-Rotating Cylinder and Airfoils," AIAA Paper 76-81, Jan. 1976.

[17]Schechenyi, E., "Supercritical Reynolds Number Simulation for Two-Dimensional Flow over Circular Cylinders," *Journal of Fluid Mechanics*, Vol. 70, Pt. 3, 1975, pp. 529–542.

[18]McLaughlin, T. E., Stephen, E. J., and Robinson, M. C., "Pressure Measurements on a Rotating Cylinder," AIAA Paper 91-3265, Aug. 1991.

[19]Dwyer, H. A., and McCroskey, W. J., "Oscillating Flow over a Cylinder at Large Reynolds Number," *Journal of Fluid Mechanics*, Vol. 61, Pt. 4, 1973, pp. 753–767.

[20]Ericsson, L. E., and Reding, J. P., "Criterion for Vortex Periodicity in Cylinder Wakes," *AIAA Journal*, Vol. 17, No. 9, 1979, pp. 1012, 1013.

[21]Yoshinaga, T., Tate, A., and Inoue, K., "Approximate Calculation of Aerodynamic Coefficients for Rotating Slender Bodies at 90 Deg Incidence," *Journal of Spacecraft and Rockets*, Vol. 19, No. 1, 1982, pp. 84–86.

[22]Ericsson, L. E., "Is Any Free Flight/Wind Tunnel Equivalence Concept Valid for Unsteady Viscous Flow?," *Journal of Aircraft*, Vol. 22, No. 10, 1985, pp. 915–919.

[23]Kamiya, N., Suzuki, S., Nakamura, M., and Yoshinaga, T., "Some Practical Aspects of the Burst of Laminar Separation Bubbles," International Council of the Aeronautical Sciences 80-10.2, Sept. 1980.

[24]Suzuki, K., and Kinoshita, T., "Characteristics of Flat Spin Unsteady Motion," 15th International Symposium on Space Technology and Science, Tokyo, May 1986.